Article

Asynchronous Broadband Signals Are the Principal Source of the BOLD Response in Human Visual Cortex

Jonathan Winawer,[1,2,*] Kendrick N. Kay,[1] Brett L. Foster,[2,3]
Andreas M. Rauschecker,[1,2,4] Josef Parvizi,[2,3]
and Brian A. Wandell[1,2]
[1]Department of Psychology
[2]Stanford Human Intracranial Cognitive Electrophysiology
Program (SHICEP)
[3]Department of Neurology & Neurological Sciences,
School of Medicine
[4]Medical Scientist Training Program and Neurosciences
Program
Stanford University, Stanford, CA 94305, USA

Summary

Background: Activity in the living human brain can be studied using multiple methods, spanning a wide range of spatial and temporal resolutions. We investigated the relationship between electric field potentials measured with electrocorticography (ECoG) and the blood oxygen level-dependent (BOLD) response measured with functional magnetic resonance imaging (fMRI). We set out to explain the full set of measurements by modeling the underlying neural circuits.
Results: ECoG responses in visual cortex can be separated into two visually driven components. One component is a specific temporal response that follows each stimulus contrast reversal ("stimulus locked"); the other component is an increase in the response variance ("asynchronous"). For electrodes in visual cortex (V1, V2, V3), the two measures respond to stimuli in the same region of visual space, but they have different spatial summation properties. The stimulus-locked ECoG component sums contrast approximately linearly across space; spatial summation in the asynchronous ECoG component is subadditive. Spatial summation measured using BOLD closely matches the asynchronous component. We created a neural simulation that accurately captures the main features of the ECoG time series; in the simulation, the stimulus-locked and asynchronous components arise from different neural circuits.
Conclusions: These observations suggest that the two ECoG components arise from different neural sources within the same cortical region. The spatial summation measurements and simulations suggest that the BOLD response arises primarily from neural sources that generate the asynchronous broadband ECoG component.

Introduction

Neuroscientists have a variety of measurement modalities available to capture neural signals from the living human brain. These modalities span a wide range of spatial and temporal resolutions, and each provides insights into distinct aspects of neural processing. The multiplicity of modalities also poses a significant challenge for developing an integrated model of brain signaling: we do not know exactly which aspect of neural signaling is captured by each modality. In this paper, we consider the relationship between two different modalities, electrocorticography (ECoG) and functional magnetic resonance imaging (fMRI).

ECoG and fMRI measure neural activity in different ways and cannot be directly compared: the ECoG signal measures the electric field potential on the cortical surface [1], whereas fMRI measures the hemodynamic blood oxygen level-dependent (BOLD) response associated with neural activity [2]. To compare such different signals, we use a stimulus-referred approach. Specifically, we compare how the ECoG and fMRI responses in visual cortex depend on the stimulus spatial position and size. Spatial position and size are important properties of visual encoding, reflected in the multiplicity of visual field maps tiling the cortex [3, 4]. We interpret the responses in the stimulus domain by calculating a population receptive field (pRF) [5–8]. The pRF defines the visual field positions of stimuli that evoke a response; we compare the pRFs (receptive field center and size) estimated from the ECoG and fMRI responses at each cortical location. Critically, we also analyze how responses to stimuli at different positions within the pRF combine to produce the full response (spatial summation).

We report three main experimental observations. First, the ECoG signal can be usefully divided into two stimulus-driven components. One component is synchronous with the flickering visual stimulus, and its temporal response rises and falls the same way with each contrast reversal (stimulus locked, or steady-state visual evoked potential [9–11]). The other component increases the response variance, but the precise temporal response changes across trials (asynchronous, or spectral perturbation [12]). Second, when analyzed using pRF methods, these two ECoG components have the same receptive field center and size, but they differ strikingly with respect to spatial summation. The stimulus-locked spatial summation is additive, whereas the asynchronous spatial summation is subadditive. Third, fMRI spatial summation is subadditive, similar to the asynchronous signal and unlike the stimulus-locked signal. Hence, the experimental data support a model in which the ECoG signal comprises at least two distinct components, and one of these components (asynchronous) matches the fMRI properties, whereas the other (stimulus locked) does not.

We created neural simulation software [13] to better understand how two neural circuits might combine to give rise to the ECoG and fMRI responses. We simulated the stimulus-locked signal as arising from the input circuitry, and the asynchronous signal as the intracortical response to the input. Modeling the signals in terms of neural circuits is an alternative to the typical approach of identifying temporal frequency bands, which have no specific biological basis, as the fundamental components. The simulations show that the fMRI response, which is mainly driven by circuitry energy consumption, will be dominated by the circuit giving rise to the asynchronous ECoG signal.

Together, the data and simulations support the view that a repetitive stimulus initiates input signals that follow the stimulus (steady-state visual evoked potential). These stimulus-locked signals induce additional, intracortical processing,

*Correspondence: winawer@stanford.edu

A

B

1 cycle

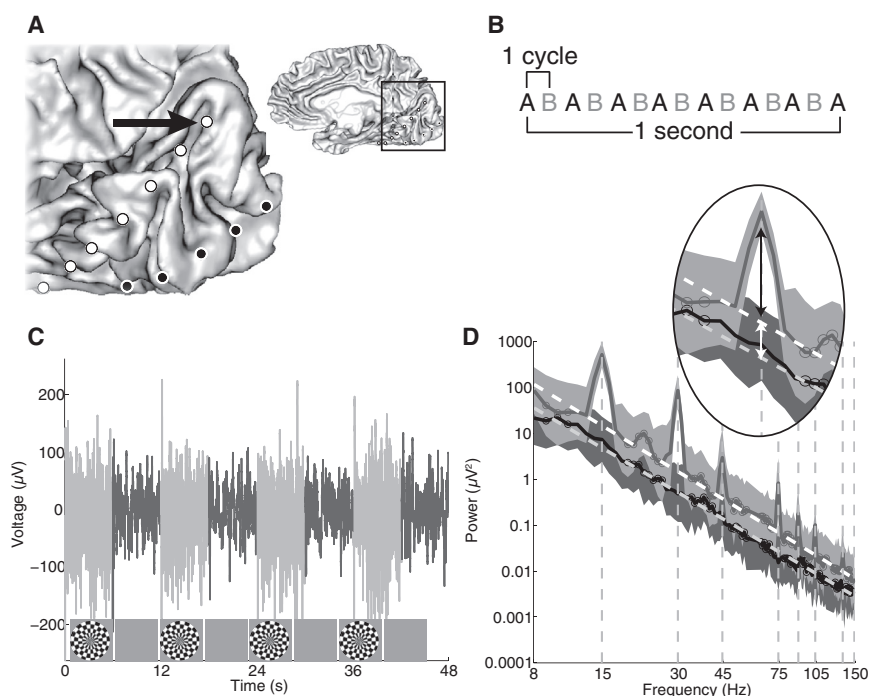A B A B A B A B A B A B A B A B A

1 second

C

D

Figure 1. Electrocorticography Signals in Visual Cortex

(A) Medial view of right occipital cortex in subject 1. The location of the magnified view is shown in the inset. The positions of two strips of intracranial electrodes are shown as white and black circles. One of the electrodes, indicated by the black arrow, is the source of the data plotted in (C) and (D).

(B) A schematic of the flicker during "on" periods. The stimulus is a dartboard pattern that reverses in contrast (pattern A to pattern B) at 7.5 Hz, such that there are 15 stimulus events per second.

(C) The ECoG time series is plotted for an "on-off" experiment (see Experimental Procedures). The "on" periods are plotted in light gray and the "off" periods in dark gray. The signal fluctuations are larger during the "on" than the "off" periods.

(D) Spectral representation of the same data plotted in (B). Short-time Fourier analysis was used to calculate the spectral power in 1 s nonoverlapping windows across the 48 s experiment. The mean spectra during the two periods differ from one another in two salient ways. First, during the "on" periods but not the "off" periods, there are spectral peaks at even harmonics of the stimulus frequency (dashed vertical lines). Second, there is a broadband elevation of the signal during "on" periods compared to "off" periods, as seen by the offset in the fitted white

lines. The broadband elevation spans the spectrum from below 10 Hz to above 150 Hz. Data at 60 and 120 Hz are not plotted because signals at these frequencies are corrupted by electrical line noise. Data points with circles indicate the points used to fit a line to the broadband signal (dashed white lines). The inset shows the responses at 15 Hz, with the arrows indicating the stimulus-locked response (black) and the broadband response (white).

See Figure S1 for example plots of the spectrum and the time series in response to a flickering contrast pattern within a bar aperture for the same electrode depicted in this figure.

which is not synchronized to the stimulus. We conclude that fMRI responses measure mainly the rise and fall of the asynchronous activity.

Results

ECoG Responses to Large-Field Flicker Reveal Two Types of Visual Signals

A simple "on-off" stimulation experiment was used to characterize ECoG responses to visual stimuli. The results of these experiments were used to develop measures for subsequent experiments investigating spatial summation. In the on-off experiments, subjects viewed large-field contrast patterns flickering at 7.5 Hz ("on" periods), interspersed with periods of zero contrast, mean luminance ("off" periods). An example of a V1 electrode and its response during an on-off experiment is shown in Figure 1. The voltage swings during the "on" periods are larger than those during the "off" periods, indicating that this channel is visually responsive (Figure 1C).

A spectral analysis of the ECoG signals (Figure 1D) reveals several characteristics that are difficult to appreciate from the time series. First, the flickering visual stimulus evokes a stimulus-locked steady-state response. This is seen in the spectral analysis as peaks at multiples of the stimulus frequency during the "on" periods [9, 10]. The large response at twice the stimulus frequency (second harmonic) indicates sensitivity to visual transients: a 7.5 Hz square-wave pattern has 15 contrast reversals per second. Across 15 visually responsive electrodes in V1, V2, and V3 (see the Supplemental Experimental Procedures section "Channel Selection" and Table S1 available online), the response power at 15 Hz increased by an average of 21.5-fold (SE = 4.7) during "on"

periods compared to "off" periods. Second, there is an increase in the broad spectral response during the "on" periods. This increase is asynchronous with the stimulus and appears as a broadband increase in the response power, spanning frequencies from below 10 Hz to above 100 Hz. The response is asynchronous in that the phases are random, and hence the voltage level is not time locked to the stimulus contrast reversals. In the time domain, this is reflected in an increase in the variance following stimulus onset. Across 15 channels, the mean broadband elevation was 2.9-fold (SE = 0.43) during "on" periods compared to "off" periods. Third, the spectral power declines with increasing frequency according to a power function, as evident by the approximately linear relationship between power and frequency when plotted on log-log axes. The power-law relationship is not caused by visual stimulation; it is observed during both the "on" and the "off" periods and is consistent with power-law spectra observed in ECoG electrodes in many parts of the brain [8, 12, 14–16].

Spatial Summation Differs between the Two ECoG Signals

In a second set of experiments, we examined spatial tuning of the ECoG signals. Subjects viewed a flickering contrast pattern through a bar aperture that made slow, discrete steps across the visual field. The responses to the moving bar, like the responses to the "on" and "off" stimuli, can be separated into stimulus-locked and asynchronous components (Figure S1). Stimuli with several bar aperture widths (Figure S1) and contrast values (Figure S2) were used to probe properties of spatial summation. For each stimulus, separate time series were constructed from the asynchronous (Figure 2A) and stimulus-locked responses (Figure 2B).
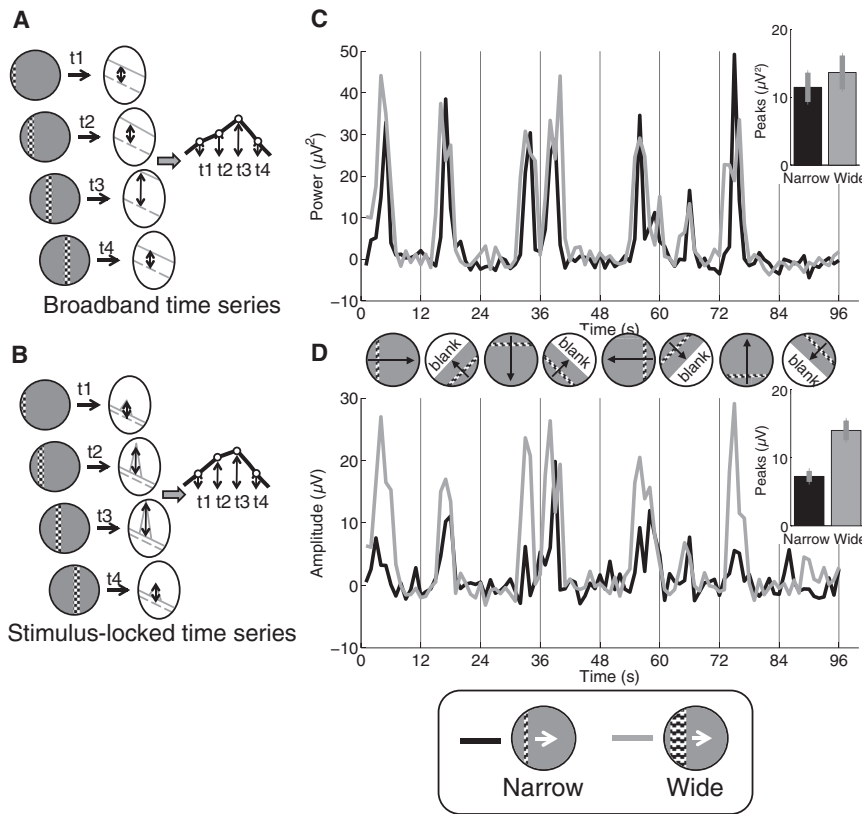
Figure 2. Spatial Summation for Broadband and Stimulus-Locked Responses

(A and B) For moving-bar experiments, each stimulus position was associated with a short time window (1 s for subjects 1, 2, 3; 0.5 s for subject 4). The Fourier transform was computed within each window, indicated in the schematics as t1, t2, t3, and t4. The power of the broadband response (A) or the amplitude of the stimulus-locked response (B) was then calculated and concatenated into a time series.

(C) Time series are shown for the broadband response to wide bar apertures (gray) and narrow bar apertures (black) for an electrode located on the V1/V2 boundary in subject 2. The bar aperture made eight sweeps across the visual field: two horizontal, two vertical, and four diagonal, indicated by the black arrows in the circular apertures. The diagonal sweeps included blank periods (white background) [6]. The mean response during the blank periods was subtracted to render a meaningful baseline level of 0 μV^2. Each sweep of the bar elicits a time series peak, except the last diagonal because the stimulus is blanked when it would cross the electrode's receptive field (lower left visual quadrant). The inset bar graph shows the mean ± SEM of the highest response during each of the eight sweeps for the narrow (black) and wide (gray) bar apertures, averaged across 15 visually responsive electrodes in V1, V2, and V3 in subjects 1, 2, and 3. See the Supplemental Experimental Procedures section "Channel Selection" and Table S1 for details on criteria used to select these 15 channels.

The peak power is about the same for the two bar aperture widths. The fact that the power does not increase much for the wide bar is not a ceiling effect, as evidenced by the fact that the response increases further when the stimulus contrast increases (Figure S2).

(D) Same as (C), but using the stimulus-locked response instead of the broadband response. The stimulus-locked peaks are higher for the wide bar aperture than the narrow bar aperture, both in the example time series and in the mean across channels (inset).

Both ECoG measures are sensitive to the position of the stimulus in the visual field (Figures 2C and 2D). The position sensitivity is reflected in the time series peaks, which arise in response to particular retinal locations of the bar apertures. The spatial trajectory of the center of the bar apertures was identical across experiments with different bar widths. The timing of the peaks is approximately the same in the four time series (two widths, two ECoG signals).

The spatial summation differs between the two types of ECoG signals. The power of the broadband signal is relatively insensitive to the stimulus width: the time series peaks for the wide and narrow bars are similar in height (Figure 2C). A different pattern is observed in the stimulus-locked time series. The time series peaks are much larger for the wide bar than the narrow bar (Figure 2D). The pattern in the example V1 time series is present across 15 visually responsive channels (Figures 2C and 2D, insets); the broadband signal increases by 21% ± 7% for the wide bars compared to the narrow bars, whereas the stimulus-locked response increases by 106% ± 22% [t(14) = 3.3; p = 0.0054, paired t test].

The time series of both ECoG components depends on the stimulus width: the response to the wider bar (Figures 2C and 2D, gray) is elevated a little longer than the response to the narrower bar (Figures 2C and 2D, black). This is presumably because there are more positions in which the wide bar overlaps the receptive fields of the neurons contributing to the electrode signals.

CSS Model Captures the Difference between the Broadband and Stimulus-Locked Responses

The pattern of broadband ECoG responses to bars of various widths suggests subadditive spatial summation. To test this idea explicitly, we fit the broadband time series and stimulus-locked time series by a population receptive field (pRF) model with compressive spatial summation (CSS model) of the form

$$r(t) = g \times \left(\int_{x,y} S(x,y,t) \times P(x,y) dx dy \right)^n, \quad \text{(Equation 1)}$$

$$P(x,y) = e^{-\left[\left((x-x_0)^2 + (y-y_0)^2 \right) / 2\sigma^2 \right]}$$

where the pRF is P(), the receptive field center is (x_0, y_0), the amplitude is scaled by a gain factor (g), and the apparent receptive field size is $\sigma/\sqrt{n}$, which corresponds to the receptive field of the response when the stimulus is a point [17].

In this model, the stimulus (S) is represented as a series of 2D contrast images, the spatial receptive field (P) is represented as a 2D circularly symmetric Gaussian, and a static nonlinearity (n; power-law function) is applied to the output (Figure 3A). When the power-law exponent is one, the model is linear, like the pRF model introduced for fMRI measurements by Dumoulin and Wandell [6]. When the exponent is less than one, the model predicts compressive (subadditive) spatial summation. The CSS model was developed to account for a range of fMRI data in visual cortex [17].

A pRF model

Stimulus Model Predicted response

B pRF center locations

Visual field position (deg)

C pRF exponent

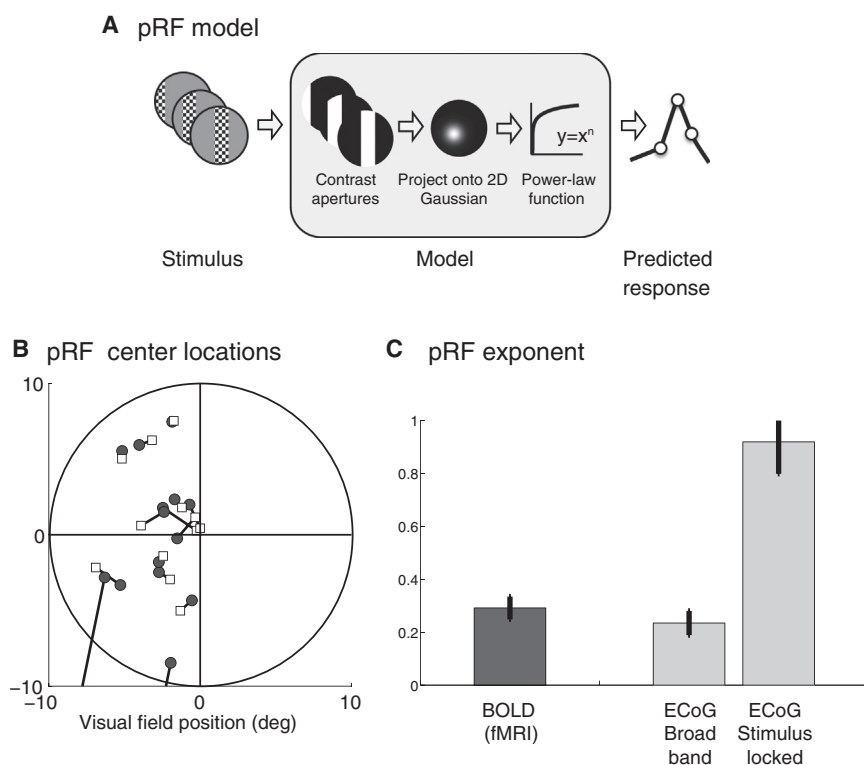BOLD (fMRI) ECoG Broad band ECoG Stimulus locked

Figure 3. Compressive Spatial Summation Model across Modalities

(A) The CSS model consists of (1) converting the stimulus into a sequence of binary contrast apertures, (2) projecting the contrast apertures onto the best-fitting 2D isotropic Gaussian population receptive field (pRF), and (3) passing the output through a static nonlinearity (power function) to predict the response. The CSS model was fit to data from V1, V2, and V3 using ECoG broadband and ECoG stimulus-locked responses (subjects 1, 2, and 3) and fMRI (subjects 5, 6, and 7).

(B) The CSS model fits to the two types of ECoG responses are shown for each electrode (lines connect results from the same electrode); the pRF center locations are similar. pRF centers are in the left visual field because subjects had electrodes in the right hemisphere.

(C) The exponent (n) from the model fits is highly compressive (n < 1) for BOLD fMRI and for ECoG broadband responses but close to linear (n ∼ 1) for the stimulus-locked response. All estimates come from model fits thresholded at 30% variance explained. For ECoG data, the plotted values represent the mean exponent ± SE across 15 electrodes in three subjects. For fMRI data, the plotted value represents the mean ± SE across three subjects, where the value for each subject was computed as the mean across three regions of interest (ROIs), and the value for each ROI was the median across voxels within the ROI. The pRF exponent and size of each of the 15 electrodes are reported in Table S2 and summarized in Figure S3.

The positions of the estimated Gaussian receptive fields are similar when measured with different signal components (Figure 3B). Across 15 electrodes in V1, V2, and V3, the eccentricity of the pRF centers measured from the two ECoG components was highly correlated (R^2 = 65%). The pRF size (Equation 1) was slightly larger for the stimulus-locked component (Figure S3; Table S2).

The power-law exponents estimated from the two ECoG responses differ: there is more spatial compression in the broadband responses than in the stimulus-locked responses (Figure 3C). The difference in compression is captured by the pRF model exponents: 0.23 ± 0.05 (broadband) and 0.92 ± 0.12 (stimulus locked), a highly significant difference between the two types of signals (t(14) = 5.5; p = 7.3 × 10^{-5}). The smaller, more compressive exponent in the fit to the broadband signal is consistent with the example V1 time series, in which the peak response does not increase as the stimulus gets larger (Figure 2C). The higher exponent in the fit to the stimulus-locked signal is consistent with the observation in the example V1 time series in which the peak response increases with stimulus width (Figure 2B). The degree of compression in the broadband model (0.23 ± 0.05) is close to the value obtained from models of fMRI voxels in V1/V2/V3 using the same range of bar widths (0.29 ± 0.04).

Cross-validated analyses confirm that the CSS model is more accurate than the linear model (exponent set to 1) for the broadband responses. Accuracy was determined via a leave-one-run-out procedure in which models were fit to two-thirds of the data (experiments with two of three bar widths) and then applied to the left-out third of the data (experiment with third bar width). For the broadband responses, the CSS model fit predicted responses better than the linear model in nearly all V1/V2/V3 electrodes (Figure 4A),

similar to the data obtained with fMRI (Figure S4). For the stimulus-locked responses, the CSS model and the linear model were equally accurate (Figure 4B). For subject 4, who was presented with static bar stimuli rather than flickering stimuli, only a broadband time series was computed; this subject shows the same pattern as the other three subjects, in which the CSS model cross-validates better than the linear model (Figure 4A, open symbols), indicating that the compressive nonlinearity evident in the broadband response is not restricted to the domain of flickering stimuli.

Compressive Spatial Summation in ECoG Broadband Is Not a Ceiling Effect

The broadband ECoG signal saturates with increasing stimulus size (Figures 2C and 3C). The assumption in the CSS model is that the saturation is due to subadditive spatial summation. An alternative explanation is that the broadband responses saturate due to a ceiling on the overall signal power. To examine this possibility, we compared responses to high-contrast stimuli to responses to low-contrast stimuli in subjects 2 and 4, for whom the bar experiments took place at low contrast (0.10% and 0.08%, respectively). For electrodes in V1, V2, and V3, for each of these subjects, the response to high-contrast stimuli was larger in each electrode than the response to low-contrast stimuli (Figure S2), indicating that the responses to the low-contrast bar stimuli used for fitting pRF models were not limited by a response ceiling.

Simulating the ECoG Temporal Responses

Several models have been proposed to simulate certain aspects of the signal dynamics of cortical neural populations [18] and electric field potentials (reviewed in [19]). These

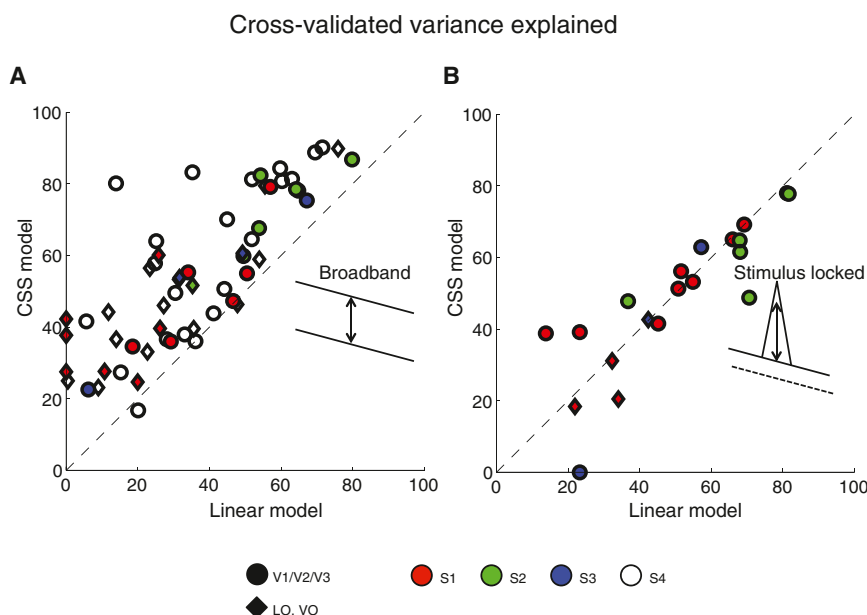## Cross-validated variance explained

Figure 4. Accuracy of CSS Model and Linear Model for Broadband and Stimulus-Locked ECoG Data

ECoG broadband responses (A) and stimulus-locked responses (B) were fit to the CSS model and a linear model. Accuracy was assessed by cross-validation. For each subject, experiments were conducted with three different bar widths. The models were fit to data from two of the experiments and then tested against the data from the left-out experiment. Plots show the variance explained for the left-out data, with each point corresponding to one electrode. For broadband responses, nearly every electrode was more accurately predicted by the CSS model than by the linear model (data points above the identity line). For stimulus-locked responses, the two types of models were equally accurate. The pattern of broadband model fits (greater accuracy for CSS model) is similar to fMRI data (Figure S4). Variance explained of less than 0 was coded as 0. S1, S2, S3, and S4 indicate subjects 1, 2, 3, and 4, respectively. LO, lateral occipital; VO, ventral occipital.

models contain two or more interacting pools of neurons, which are driven by both external signals and signals between the pools. Even relatively simple models, in which neural responses are driven only by external signals, can capture important features of electric field potential dynamics, such as power-law scaling of the spectral power as a function of frequency [20, 21].

We implemented a specific version of these models that captures the full dynamics of the ECoG measurements described here [13]. The simulation is based on the principle that two circuits contribute to the mean field potential measured by the ECoG signal. We assume that these are distinct circuits because the spatial summation properties differ between the stimulus-locked and broadband responses.

The stimulus-locked and broadband circuit simulations share certain similarities. In both cases, a Poisson spiking process initiates the circuit responses. These spikes drive a mixture of excitatory and inhibitory synapses. The synaptic weights are selected randomly and sum to zero. The post-synaptic responses are generated through a mechanism described by Miller et al. (Equations 3 and 4 in [20]), and the parameters are the same. Spikes initiate a dendritic current that rises rapidly and decays exponentially. A leaky integrator accumulates charge across many synapses, and the charge is lost ohmically across the dendritic membranes. The ECoG signal is assumed to be proportional to this transmembrane current, and the total time-varying ECoG response is the sum of the responses from the two circuits.

The two circuits differ in their parameters and organization. The broadband circuit is initiated by a Poisson process with a spike rate that steps between two levels; the level depends only on the presence or absence of the flickering stimulus. We do not model the broadband power as rising and falling within the short period of time between each contrast reversal because we do not observe such coupling in the data; if the flicker rate were much slower, then it might be necessary to model the broadband response as increasing and then saturating with each stimulus event, rather than stepping between two discrete levels. Because there are an equal number of

excitatory and inhibitory synapses, the time course of the mean electrical field potential from the broadband circuit fluctuates around zero. The stimulus-locked response is initiated by two time-varying Poisson processes whose rate is time locked to contrast reversals in the stimulus. The two inputs separately target excitatory and inhibitory synapses. The excitatory and inhibitory inputs are slightly offset in time. Because the inhibitory input is delayed by 25 ms, the electrical field response arising from the stimulus-locked circuit is biphasic.

The simulated time series captures the main aspects of the data (Figure 5). First, the simulation correctly models the power-law relation between power and frequency. Second, it captures the broadband response elevation when the stimulus is present. Third, the simulation captures the narrow band peaks at even harmonics of the stimulus frequency (15 Hz, 30 Hz, and so on). These peaks are the largest visible feature of the spectral plots and the time series; the response peaks correspond to the checkerboard contrast reversal times (15 times per second). The simulation does not attempt to capture the phase of the stimulus-locked response, because the phase was observed to differ substantially between electrodes; this is expected if response latency differs across visual field maps and visual field positions. Finally, the model captures the fact that the power of the stimulus-locked peaks is changed very little by response averaging (light red versus dark red peaks in Figure 5, lower plots; see also Figure S5). The asynchronous broadband response, however, does decline with averaging. The difference arises because the phase of the stimulus-locked response is the same across trials, whereas the phases of the broadband frequency terms are distributed randomly.

Discussion

Dissecting Field Potentials in Human Visual Cortex

We separated the ECoG responses from human visual cortex into a stimulus-locked response and an asynchronous response that is broadband. We estimated the pRF properties of these two responses. The responses agree in their
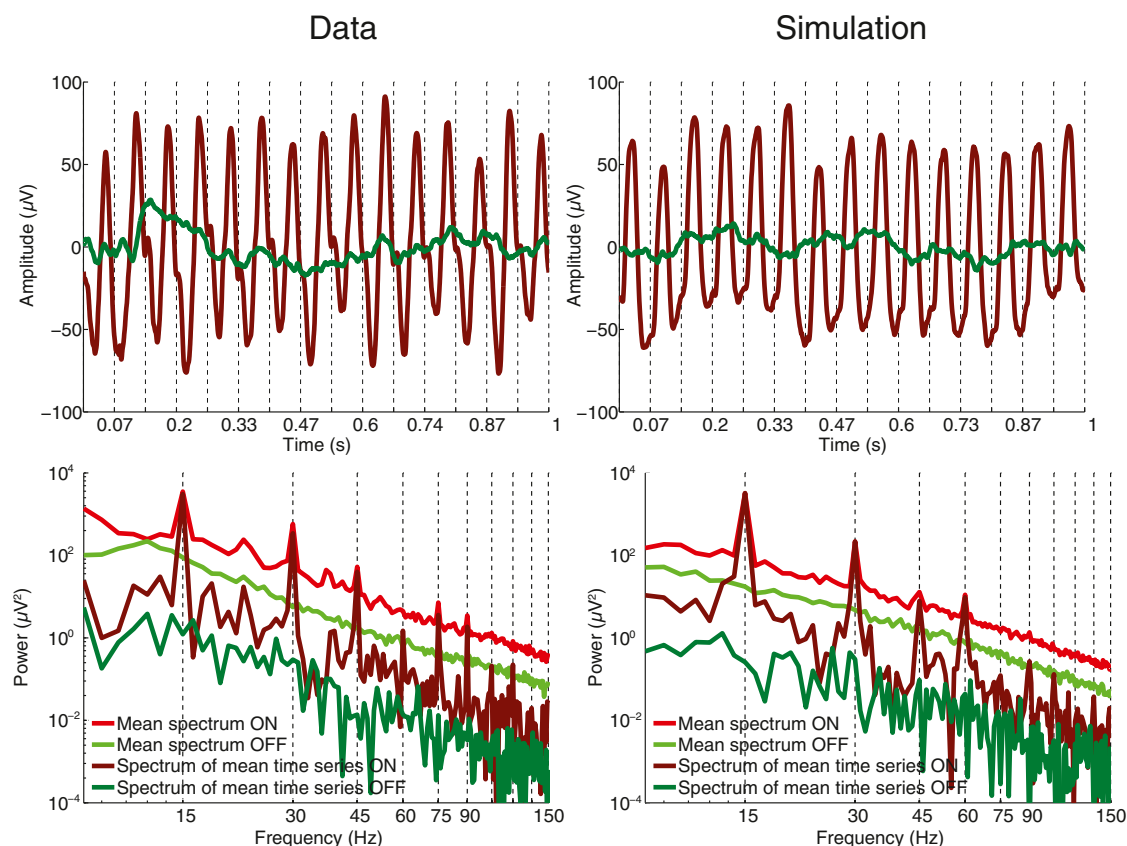
Figure 5. Quantitative Model of the ECoG Responses

The left plots show ECoG responses from a V1 electrode in subject 1 from responses to a large-field flickering grating ("on"; red) or a zero-contrast, mean luminance screen ("off"; green). The right plots show a simulation of responses to the same stimuli. The upper plots show the average time series from 72 1 s recording blocks. The lower plots show the average spectral responses (bright red and green) and the spectra of the average time series (dark red and green). The broadband response in the model and the data decreases significantly if the data are averaged in the time domain; the stimulus-locked response does not decrease substantially with averaging in the time domain. This observation is further quantified in Figure S5.

estimates of the pRF center positions and the region of the visual field that evokes a response (pRF size).

The two ECoG responses differ, however, with respect to spatial summation. The stimulus-locked response amplitude increases continuously as the stimulus covers more of the pRF, reaching a maximum response when the stimulus covers the full pRF. The asynchronous activity reaches its maximum response when the stimulus covers only a portion of the pRF. The differences in spatial summation between the stimulus-locked and asynchronous responses suggest that these responses arise from different neural sources.

Simulating the Neural Circuits
The circuitry simulation begins with a Poisson input, representing the spikes arriving to cortex; the simulation generates a continuous voltage output, representing the ECoG response [13]. The simulation models two neural circuits that each make a distinct contribution. The stimulus-locked circuit gives rise to a periodic oscillation in the time domain, which is localized in the frequency domain. The asynchronous responses give rise to a general increase in response variance in the time domain that is broadband in the frequency domain. The model fits the data quite closely without assigning a functional role to specific frequency bands. The functional role is assigned to the circuits and their properties.

Electrophysiological measurements on the cortical surface show that visual stimulation gives rise to a response that arises first in a small region and then spreads as a traveling wave [22, 23]. We were prompted to consider the implications of this traveling wave in the simulation and measurements, and in particular to understand whether the traveling wave might explain the subadditivity of spatial summation. The wave produces a response in which different cortical points respond at different phases (incoherence); sufficiently large temporal incoherence predicts subadditivity of spatial summation. In Figure S6, we show that there is a very small phase difference, consistent with the electrophysiological measurements. However, the incoherence arising from the traveling wave is far too small to explain the observed spatial summation subadditivity. We include simulations that exclude this explanation of spatial summation subadditivity ([13] and Figure S6).

Broadband and Stimulus-Locked Spatial Summation
The simulation captures the ECoG time series, but it does not model the spatial summation of signals. To explain the difference in spatial summation between stimulus-locked and broadband ECoG responses, we suggest an informal model (Figure 6). The idea is that the difference arises from the cortical spread of the responses from these circuits. The
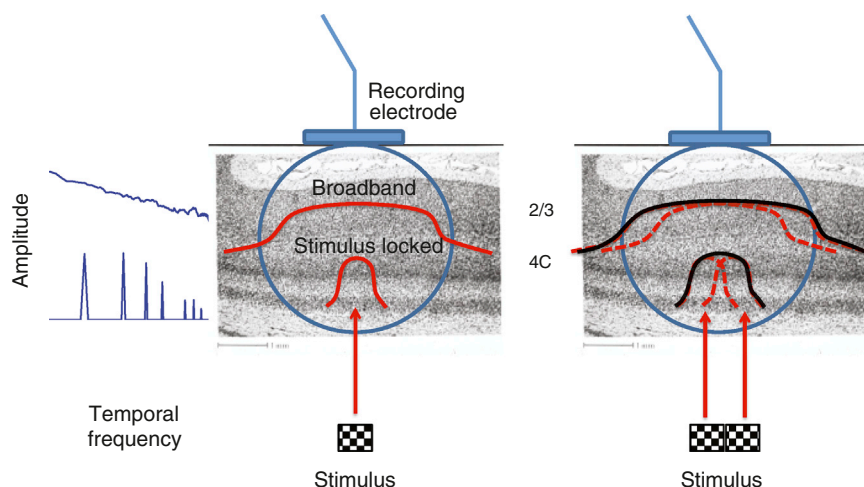
Figure 6. Visualization of a Possible Spatial Distribution of the ECoG Signal Sources

According to this model, inputs from a narrow stimulus (left) give rise to a stimulus-locked response in a relatively small region of cortical input layers; when the stimulus is wider (right), the stimulus-locked response is correspondingly larger. When the response from neighboring stimulus locations gives rise to responses in overlapping cortical locations (dashed red lines), we assume that the total neural response is approximately the maximum of the two responses (black lines). The stimulus-locked responses measured by the electrode grow with stimulus size because the area of cortical stimulation under the electrode increases with stimulus size. In contrast, the broadband response from a small stimulus already spans the electrode antenna function. Consequently, the wider stimulus does not produce a much larger response in the electrode than the narrow stimulus. Alternative explanations for why the wider bar could produce a larger response are schematized in Figure S6.

difference in spread produces a significant difference in the signal picked up by the implanted electrodes.

Specifically, we propose that the cortical inputs are narrowly confined in space, possibly at the input layers. These inputs induce asynchronous activity in the superficial layers of cortex that spreads more widely (Figure 6, left panel; Figure S6) [24]. When the response from neighboring stimulus locations gives rise to responses in overlapping locations, we assume that the total neural response is approximately the maximum of the responses. This model suggests that the stimulus-locked response will grow linearly with bar width: increasing the spatial area of the input spreads the stimulus-locked response across the measurement field of the electrode. The asynchronous broadband responses are spread so that even the thin bars produce a relatively wide response; increasing the spatial area or amplitude of the input does not increase the broadband response within the measurement field of the electrode.

This model is qualitatively consistent with measurements of cortical activity using voltage-sensitive dyes [24, 25]. The same authors report that the response to a small stimulus that evokes activity within a 1 mm^2 region of the input layers evokes activity that quickly spreads over 10 mm^2 in the superficial layers (Figure 17 in [26]). Similar to the asynchronous broadband ECoG signal, the voltage-sensitive dye measurements in the superficial layers reflect subadditive spatial summation (Figure 13 in [26]).

Field Potentials and fMRI Responses

The spatial summation characteristics of the fMRI response correspond to the characteristics of the broadband response, not those of the stimulus-locked response. This might appear surprising, given that the largest amplitude of the ECoG signal is stimulus locked (Figures 1 and S1). To understand why, note that the response power of a signal that is the sum of N independent sources grows as N^2 when the sources are synchronous, but the broadband response power only grows as N when the sources are asynchronous. Thus, the same number of sources, each presumably consuming equal amounts of energy, generates a larger signal when they are stimulus locked compared to the signal generated by asynchronous signals in random phase relationships. This pattern is evident in the simulation: the number of spikes that drive the stimulus-locked response is about ten times smaller than

the number of spikes that drive the broadband response, even though the stimulus-locked signal is quite high in the simulated time series (see simulation code in [13] for plots of the spike levels driving each response).

Hence, the fMRI response—which depends on energy consumption—may be largely determined by the broadband response [2, 27, 28]. This does not imply that the stimulus-locked response fails to influence the fMRI response or is always immeasurable; it may prove possible to isolate the portion of the fMRI response driven by the evoked response component by using specific stimulus manipulations. Nor does it imply that narrowband responses that are not stimulus locked, such as beta rhythms in motor cortex [27] or alpha rhythms in visual cortex [8], cannot exert some influence on the fMRI response.

Where Is Narrowband Gamma?

The broadband response spans the temporal frequency range that is often described as gamma band (30–80 Hz) and high gamma (80–150 Hz). Some investigators measuring electrical field responses in visual cortex observe a high-amplitude, narrowband response in this range (reviewed in [29]) The peak frequency depends on intrinsic properties of the cortex such as the density of gamma-aminobutyric acid (GABA) [30] as well as stimulus characteristics such as contrast and stimulus size [31]. Several investigators have shown that this narrowband peak is present for simple grating stimuli, but not for other similar stimuli. For example, the peak is reduced or eliminated by the introduction of a second grating [32, 33] or superimposed white noise [34] and is absent for low to moderate stimulus contrasts [35]. Importantly, a broadband spectral elevation has been shown in several of these stimulus configurations that eliminate the narrowband gamma peak [33, 35]. We confirm this because for the checkerboard patterns we used, there are no narrowband peaks other than the stimulus-locked peaks. In pilot experiments, we have seen narrowband peaks for grating stimuli. Because the properties and even existence of the narrowband peak in these early visual areas are dependent on spatial properties of the stimulus, the peak is probably not an essential requirement for seeing. The circuit properties that give rise to the peak may differ from those that give rise to the broadband response [35, 36].

Circuit Models

The association between specific electrical rhythms and physiological states is an important tradition [37]. Decomposing ECoG and local field potential responses into different frequency bands builds on this tradition, making it natural to ask whether a particular frequency band is particularly predictive of the BOLD response. A number of investigators have used this approach and observed that the response levels in certain frequency bands, particularly in the range from 30 to 100 Hz, are more highly correlated with the hemodynamic response [38–43].

In this paper, we propose a different analysis of the ECoG signal. Rather than decomposing the ECoG signal into frequency bands, we model the signal as arising from two neural circuits. The response of one circuit is stimulus locked, tracking the rapid stimulus contrast reversals; the response of the second circuit is asynchronous, fluctuating more through multiple contrast reversals.

The decomposition into neural circuit models is motivated by the data: the ECoG responses to the visual stimuli naturally separate into two types. But these types do not correspond to distinct frequency bands: the model contains two circuits that contribute to overlapping frequency bands. The circuits are better understood as a brief, transient response to contrast, followed by a longer, sustained response that spans several of these transient periods.

Conclusions

Both ECoG and fMRI responses to a range of contrast patterns were examined using a model-based approach. A pRF model, consisting of linear spatial summation followed by a pointwise nonlinearity, accurately characterizes the spatial summation properties of the BOLD response and two components (stimulus locked and broadband) of the ECoG response. Consistent with prior work, model fits to the BOLD signal indicate a significantly compressive spatial nonlinearity. The broadband ECoG response is similarly described by a compressive nonlinearity, in quantitative agreement with fMRI measurements. The stimulus-locked ECoG response has approximately linear spatial summation, indicating that this component of the ECoG response arises from different network activity than that underlying the broadband ECoG and the BOLD responses.

We implemented a network model to capture the properties of the ECoG temporal response. The amplitude of the stimulus-locked response is a very large fluctuation in the gross electric potential in the ECoG electrode. But simulations suggest that this response likely arises from a relatively small population of stimulus-locked neurons and that most of the energy in the model is consumed by the neurons driving the broadband responses. The energy analysis and the shared spatial summation characteristics suggest that the BOLD response is mainly driven by the same sources that carry the broadband ECoG responses.

Experimental Procedures

Further details of the experimental procedures can be found in the Supplemental Experimental Procedures.

Participants

ECoG data were collected from four clinical volunteers (two males, two females; ages 41–57; subjects 1–4). Three additional participants took part in fMRI experiments (all males; ages 25–39; subjects 5–7). Informed written consent was obtained from all participants, and all protocols were approved by the Stanford University Institutional Review Board.

Stimuli for ECoG Experiments
Bar Stimuli

For subjects 1, 2, and 3, bar experiments were similar to those used previously for fMRI experiments [6, 44, 45]. A contrast pattern was viewed through a bar aperture that swept across the visual field eight times in twelve 1 s steps (see Figure 2 for the sequence). For each of these three participants, there were separate experiments with different bar widths (1/16, 1/8, and 1/4 the maximum bar height). For subjects 2 and 3, the contrast of the checkerboard pattern within the moving bars was 78%, the maximum afforded by the display given the ambient illumination in the hospital room. For subjects 1 and 4, the contrast was reduced to 10% and 8%, respectively, to avoid the possibility of saturation in the ECoG responses. For subject 4, bar stimuli were presented as static images for 100 ms (no flicker), in random order (rather than as sweeps across the visual field), with a 400 ms mean luminance interval between stimuli.

Large-Field On-Off Stimuli

Large-field on-off stimuli consisted of a circular aperture (largest circle that fit completely within the display) and a contrast-reversing dartboard pattern (7.5 Hz square wave). Experiments consisted of four 6 s "on" periods alternated with four 6 s "off" periods. During the "off" periods, the screen was blank (mean luminance of the contrast pattern) except for a fixation dot.

Stimuli for fMRI Experiments
Bar Stimuli

The bar stimuli used in fMRI experiments with control subjects were the same as those used in ECoG experiments except for three differences: the duration of each aperture position was 1.5 s rather than 1 s, the number of discrete steps in one sweep of the visual field was 16 rather than 12, and the contrast pattern within the aperture drifted rather than flickered (2 Hz temporal frequency) (see [6] and [44]). For each subject, there were nine bar experiments, three with each of three bar widths. Bar stimuli for ECoG subjects were used only to identify visual field maps, not to assess spatial summation. Hence, only one bar width was used—1/8 the length of the bar—the same as the middle width used in control subject fMRI experiments and in ECoG experiments.

Broadband and Stimulus-Locked ECoG Responses

The time series of the broadband and stimulus-locked responses to bar stimuli were constructed by short-time Fourier analysis. The window for Fourier analysis was the duration that a stimulus aperture remained in a position (1 s for subjects 1, 2, and 3; 0.5 s for subject 4). The time series from the 1 s window was multiplied by a Hann window (raised cosine) to reduce edge artifacts.

For the broadband data, a line was fit in log-log space to the signal power (squared amplitude) of Fourier components from 8 to 150 Hz, excluding values within 2 Hz of even harmonics of the stimulus frequency (15, 30, 45, 60, 75, 90, 105, 120, 135, and 150 Hz) (Figure 1D). The slope of the line was forced to be the same for all stimulus positions for a given electrode. The height of the line at 15 Hz was taken as the broadband signal for that time point. The stimulus-locked signal was defined as the amplitude at 15 Hz, after subtracting the broadband fit. Calculations were also run on the stimulus-locked time series omitting the subtraction of the broadband fit; the pattern of effects is unchanged, with only a small change in the parameter values.

Simulation of the ECoG Temporal Responses

We implemented software to simulate the main features of the ECoG responses. The principles and simulations are described in Results. The full MATLAB code implementing the simulation, including examples and the code needed to reproduce the simulation in Results, is available in [13].

Supplemental Information

Supplemental Information include six figures, two tables, and Supplemental Experimental Procedures and can be found with this article online at http://dx.doi.org/10.1016/j.cub.2013.05.001.

Acknowledgments

References

1. Buzsáki, G., Anastassiou, C.A., and Koch, C. (2012). The origin of extracellular fields and currents—EEG, ECoG, LFP and spikes. Nat. Rev. Neurosci. *13*, 407–420.

2. Logothetis, N.K., and Wandell, B.A. (2004). Interpreting the BOLD signal. Annu. Rev. Physiol. *66*, 735–769.

3. Wandell, B.A., Dumoulin, S.O., and Brewer, A.A. (2007). Visual field maps in human cortex. Neuron *56*, 366–383.

4. Wandell, B.A., and Winawer, J. (2011). Imaging retinotopic maps in the human brain. Vision Res. *51*, 718–737.

5. Victor, J.D., Purpura, K., Katz, E., and Mao, B. (1994). Population encoding of spatial frequency, orientation, and color in macaque V1. J. Neurophysiol. *72*, 2151–2166.

6. Dumoulin, S.O., and Wandell, B.A. (2008). Population receptive field estimates in human visual cortex. Neuroimage *39*, 647–660.

7. Yoshor, D., Bosking, W.H., Ghose, G.M., and Maunsell, J.H. (2007). Receptive fields in human visual cortex mapped with surface electrodes. Cereb. Cortex *17*, 2293–2302.

8. Harvey, B.M., Vansteensel, M.J., Ferrier, C.H., Petridou, N., Zuiderbaan, W., Aarnoutse, E.J., Bleichner, M.G., Dijkerman, H.C., van Zandvoort, M.J., Leijten, F.S., et al. (2013). Frequency specific spatial interactions in human electrocorticography: V1 alpha oscillations reflect surround suppression. Neuroimage *65*, 424–432.

9. Regan, D. (1966). Some characteristics of average steady-state and transient responses evoked by modulated light. Electroencephalogr. Clin. Neurophysiol. *20*, 238–248.

10. Norcia, A.M., and Tyler, C.W. (1985). Spatial frequency sweep VEP: visual acuity during the first year of life. Vision Res. *25*, 1399–1408.

11. Van Der Tweel, L.H., and Lunel, H.F. (1965). Human visual responses to sinusoidally modulated light. Electroencephalogr. Clin. Neurophysiol. *18*, 587–598.

12. Miller, K.J., Zanos, S., Fetz, E.E., den Nijs, M., and Ojemann, J.G. (2009). Decoupling the cortical power spectrum reveals real-time representation of individual finger movements in humans. J. Neurosci. *29*, 3132–3137.

13. Winawer, J., Kay, K.N., Foster, B.L., Rauschecker, A.M., Parvizi, J., and Wandell, B.A. (2013). Stanford Digital Repository: Code and data supplement for "Asynchronous broadband signals are the principal source of the BOLD response in human visual cortex." http://purl.stanford.edu/hj582pj3902.

14. Manning, J.R., Jacobs, J., Fried, I., and Kahana, M.J. (2009). Broadband shifts in local field potential power spectra are correlated with single-neuron spiking in humans. J. Neurosci. *29*, 13613–13620.

15. Honey, C.J., Thesen, T., Donner, T.H., Silbert, L.J., Carlson, C.E., Devinsky, O., Doyle, W.K., Rubin, N., Heeger, D.J., and Hasson, U. (2012). Slow cortical dynamics and the accumulation of information over long timescales. Neuron *76*, 423–434.

16. Kunii, N., Kamada, K., Ota, T., Kawai, K., and Saito, N. (2013). Characteristic profiles of high gamma activity and blood oxygenation level-dependent responses in various language areas. Neuroimage *65*, 242–249.

17. Kay, K.N., Winawer, J., Mezer, A., and Wandell, B.A. (2013). Compressive spatial summation in human visual cortex. J. Neurophysiol. Published online April 24, 2013. http://dx.doi.org/10.1152/jn.00105.2013.

18. Wilson, H.R., and Cowan, J.D. (1972). Excitatory and inhibitory interactions in localized populations of model neurons. Biophys. J. *12*, 1–24.

19. Liley, D.T.J., Foster, B.L., and Bojak, I. (2012). Co-operative populations of neurons: Mean field models of mesoscopic brain activity. In Computational Systems Neurobiology, N. Le Novère, ed. (Dordrecht: Springer), pp. 317–364.

20. Miller, K.J., Sorensen, L.B., Ojemann, J.G., and den Nijs, M. (2009). Power-law scaling in the brain surface electric potential. PLoS Comput. Biol. *5*, e1000609.

21. Milstein, J., Mormann, F., Fried, I., and Koch, C. (2009). Neuronal shot noise and Brownian 1/f2 behavior in the local field potential. PLoS One *4*, e4338.

22. Benucci, A., Frazor, R.A., and Carandini, M. (2007). Standing waves and traveling waves distinguish two circuits in visual cortex. Neuron *55*, 103–117.

23. Sato, T.K., Nauhaus, I., and Carandini, M. (2012). Traveling waves in visual cortex. Neuron *75*, 218–229.

24. Palmer, C.R., Chen, Y., and Seidemann, E. (2012). Uniform spatial spread of population activity in primate parafoveal V1. J. Neurophysiol. *107*, 1857–1867.

25. Grinvald, A., and Hildesheim, R. (2004). VSDI: a new era in functional imaging of cortical dynamics. Nat. Rev. Neurosci. *5*, 874–885.

26. Grinvald, A., Lieke, E.E., Frostig, R.D., and Hildesheim, R. (1994). Cortical point-spread function and long-range lateral interactions revealed by real-time optical imaging of macaque monkey primary visual cortex. J. Neurosci. *14*, 2545–2568.

27. Hermes, D., Miller, K.J., Vansteensel, M.J., Aarnoutse, E.J., Leijten, F.S., and Ramsey, N.F. (2012). Neurophysiologic correlates of fMRI in human motor cortex. Hum. Brain Mapp. *33*, 1689–1699.

28. Engell, A.D., Huettel, S., and McCarthy, G. (2012). The fMRI BOLD signal tracks electrophysiological spectral perturbations, not event-related potentials. Neuroimage *59*, 2600–2606.

29. Fries, P., Nikolić, D., and Singer, W. (2007). The gamma cycle. Trends Neurosci. *30*, 309–316.

30. Muthukumaraswamy, S.D., Edden, R.A., Jones, D.K., Swettenham, J.B., and Singh, K.D. (2009). Resting GABA concentration predicts peak gamma frequency and fMRI amplitude in response to visual stimulation in humans. Proc. Natl. Acad. Sci. USA *106*, 8356–8361.

31. Ray, S., and Maunsell, J.H. (2010). Differences in gamma frequencies across visual cortex restrict their possible use in computation. Neuron *67*, 885–896.

32. Bartolo, M.J., Gieselmann, M.A., Vuksanovic, V., Hunter, D., Sun, L., Chen, X., Delicato, L.S., and Thiele, A. (2011). Stimulus-induced dissociation of neuronal firing rates and local field potential gamma power and its relationship to the resonance blood oxygen level-dependent signal in macaque primary visual cortex. Eur. J. Neurosci. *34*, 1857–1870.

33. Lima, B., Singer, W., Chen, N.H., and Neuenschwander, S. (2010). Synchronization dynamics in response to plaid stimuli in monkey V1. Cereb. Cortex *20*, 1556–1573.

34. Zhou, Z., Bernard, M.R., and Bonds, A.B. (2008). Deconstruction of spatial integrity in visual stimulus detected by modulation of synchronized activity in cat visual cortex. J. Neurosci. *28*, 3759–3768.

35. Henrie, J.A., and Shapley, R. (2005). LFP power spectra in V1 cortex: the graded effect of stimulus contrast. J. Neurophysiol. *94*, 479–490.

36. Ray, S., and Maunsell, J.H. (2011). Different origins of gamma rhythm and high-gamma activity in macaque visual cortex. PLoS Biol. *9*, e1000610.

37. Basar, E., and Bullock, T.H. (1992). Induced Rhythms in the Brain (Boston: Birkhäuser).

38. Goense, J.B., and Logothetis, N.K. (2008). Neurophysiology of the BOLD fMRI signal in awake monkeys. Curr. Biol. *18*, 631–640.

39. Niessing, J., Ebisch, B., Schmidt, K.E., Niessing, M., Singer, W., and Galuske, R.A. (2005). Hemodynamic signals correlate tightly with synchronized gamma oscillations. Science *309*, 948–951.

40. Mukamel, R., Gelbard, H., Arieli, A., Hasson, U., Fried, I., and Malach, R. (2005). Coupling between neuronal firing, field potentials, and FMRI in human auditory cortex. Science *309*, 951–954.

41. Shmuel, A., Augath, M., Oeltermann, A., and Logothetis, N.K. (2006). Negative functional MRI response correlates with decreases in neuronal activity in monkey visual area V1. Nat. Neurosci. *9*, 569–577.

42. Logothetis, N.K., Pauls, J., Augath, M., Trinath, T., and Oeltermann, A. (2001). Neurophysiological investigation of the basis of the fMRI signal. Nature *412*, 150–157.

43. Lachaux, J.P., Fonlupt, P., Kahane, P., Minotti, L., Hoffmann, D., Bertrand, O., and Baciu, M. (2007). Relationship between task-related gamma oscillations and BOLD signal: new insights from combined fMRI and intracranial EEG. Hum. Brain Mapp. *28*, 1368–1375.

44. Winawer, J., Horiguchi, H., Sayres, R.A., Amano, K., and Wandell, B.A. (2010). Mapping hV4 and ventral occipital cortex: the venous eclipse. J. Vis. *10*, 1.

45. Amano, K., Wandell, B.A., and Dumoulin, S.O. (2009). Visual field maps, population receptive field sizes, and visual field coverage in the human MT+ complex. J. Neurophysiol. *102*, 2704–2718.